CCS Chemistry

COMMUNICATION

Received: Feb. 5, 2024 | Accepted: Mar. 21, 2024 | Published: Apr. 11, 2024

Characterization and Monitoring of Transient Enamine Radical Intermediates in Photoredox/Chiral Primary Amine Synergistic Catalytic Cycle

Shixue Zhang[†], Liang Cheng[†], Jian-Qing Qi[†], Zongbin Jia, Long Zhang, Lei Jiao*, Xingwei Guo* & Sanzhong Luo*

Center of Basic Molecular Science (CBMS), Department of Chemistry, Tsinghua University, Beijing 100084

**Corresponding authors: leijiao@mail.tsinghua.edu.cn; xingwei_guo@mail.tsinghua.edu.cn; luosz@tsinghua.edu.cn;*
[†]S. Zhang, L. Cheng, and J.-Q. Qi contributed equally to this work.

Cite this: *CCS Chem*. **2024**, Just Published. DOI: 10.31635/ccschem.024.202404035

Enamine-derived radicals are crucial intermediates in singly occupied molecular orbital (SOMO) catalysis. However, observing them directly is elusive and remains a long-standing challenge. Here, an advanced time-resolved electron paramagnetic resonance technique was employed to characterize and monitor the key intermediates in photoredox transformations by primary aminocatalysis on a microsecond timescale. The transient enamine radical cation, generated by single electron transfer (SET), and the deprotonated form of α-imino radical intermediates were directly observed for the first time, both spectroscopically and kinetically. In reactions with styrene, enamine radical cation was found to be faster than α-imino radical by one order of magnitude. This revealed the subtle role of deprotonation associated with secondary enamine radical cation in the photoredox transformations by primary aminocatalysis.

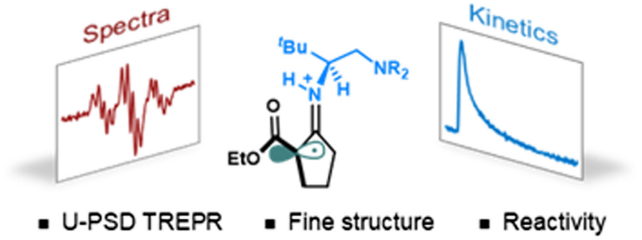

Keywords: **aminocatalysis, radical chemistry, electron paramagnetic resonance, direct observation, time-resolved technique**

Introduction

Enamine, being an electron-rich species, possesses inherent nucleophilicity and finds extensive applications in various α-functionalization reactions of carbonyl compounds.[1–3] Apart from the conventional approach involving activation of the highest occupied molecular orbital (HOMO), enamine exhibits remarkable redox properties and can undergo facile oxidation through single electron transfer (SET) processes to form enamine radical cation. This open-shell intermediate can be engaged in various coupling reactions, serving as the foundation for the development of singly occupied molecular orbital (SOMO) catalysis, as pioneered by MacMillan and coworkers[4–11] and further developed by others.[12–16] Over the past decade, a diverse array of SOMO-based transformations of enamines, including alkylation,[5,11,17] allylic alkylation,[4,10] and arylation,[9,18] have been successfully established (Figure 1a). We have made much progress in practicing SOMO catalysis with primary amine

Citation: *CCS Chem.* **2024**, Just Published. DOI: 10.31635/ccschem.024.202404035
Link to VoR: https://doi.org/10.31635/ccschem.024.202404035

catalysts.[19–27] Despite the remarkable synthetic value of these transformations, direct observation of the key SOMO radical intermediate is still quite limited. By using mass spectroscopy, Engeser and coworkers[28] detected the enamine radical cation under chemical oxidation conditions, supporting the existence of α-imino radical-type intermediate by a SET of an enamine. However, to date, there still lacks direct evidence for the in situ formation of these proposed transient radical intermediates under synthetic conditions, especially under typical photoredox conditions. Moreover, the elucidation of their fine structure and reactivity remains impossible. We believe that detailed spectroscopic characterization of the key radical intermediate involved in photoredox catalytic SOMO-activation of enamines, as well as elucidating its reactivity would be of great value.

In previous studies, we showcased a C–H dehydrogenative allylic alkylation between β-ketoesters and styrenes employing a ternary catalytic system comprising a chiral primary amine, a photoredox catalyst, and a cobaloxime cocatalyst (Figure 1b).[24] In this transformation, the enamine generated from the chiral primary amine catalyst and the β-ketoester was believed to be the key intermediate. It was proposed that the enamine intermediate was engaged in SET with the Ir catalyst, leading to the formation of an enamine radical cation and an ester substituted α-imino radical intermediate, which were responsible for the observed SOMO reactivity. However, despite many devoted experimental efforts, these intermediates have not been directly observed experimentally, hampering a deeper understanding of the catalytic system.

Recently, we developed an advanced time-resolved electron paramagnetic resonance (TREPR) technique, named the ultrawide single sideband phase-sensitive detection (U-PSD) TREPR.[29] This technique is particularly suitable for detecting weak signals of transient radicals under near synthetic conditions, providing a first-derivative EPR spectrum with a high time resolution. By applying the U-PSD TREPR, we were able to directly observe the enamine radical cation and α-imino radical intermediates involved in the chiral primary amine-catalyzed allylation of β-ketoesters for the first time. The acquired TREPR spectra and kinetic profiles allowed us to confirm the authentic identity of the chiral radicals and quantify their reactivities, clarifying the structure-activity relationships of these transient intermediates.

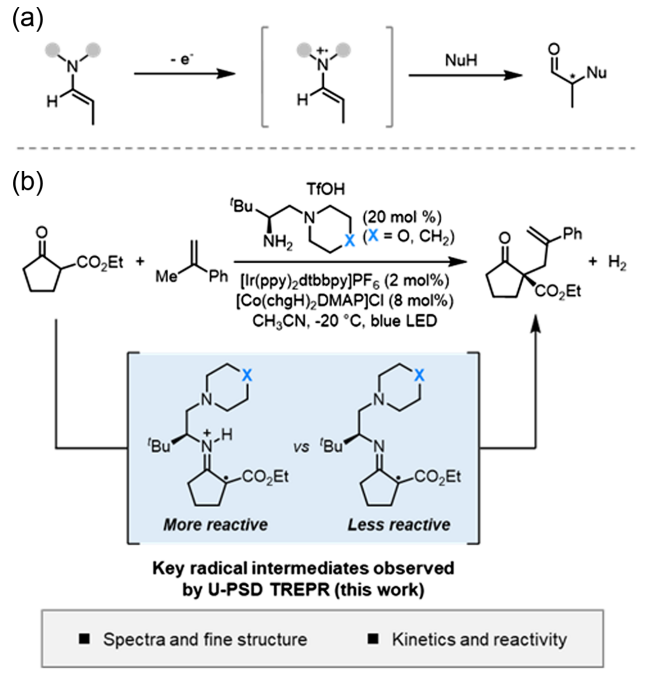

Figure 1 | *Formation and reactivity of α-imino radical intermediates. (a) General mechanistic scheme. (b) This work.*

Results and Discussion

We chose the preformed enamines **1-3**, condensed from primary amines **A1-A3** and ethyl cyclopentanone-2-carboxylate as our model substrates. The sample solutions containing $[Ir(ppy)_2(dtbbpy)]PF_6$ ([Ir]) and preformed enamines **1-3** were subjected to U-PSD TREPR measurements, as described in our previous works.[29] The radical of interest was generated through the photoinduced electron transfer between the [Ir] and the enamine substrate with an ns-pulsed optical parametric oscillators (OPO) laser system operating at an excitation wavelength of 450 nm (Figure 2a).

We first used enamine **1** as the substrate, and gained a clear TREPR spectrum by integrating 0–2 μs after laser pulses (Figure 2b), showing a well-resolved splitting pattern (a(N) = 0.57 mT, a(H) = 0.23 mT, a(H) = 0.64 mT, 2a(H) = 3.44 mT). The hyperfine splittings (HFSs) obtained from this spectrum agree well with the density functional theory (DFT) computational results (Figure 2c). The large HFS from H^1 (compared to β–H in cyclopentyl radical)[30] and the small HFS from N (compared to N atom in planar amine radical cation)[31] indicated that the unpaired electron was mainly populated on the α-carbonyl carbon atom, which was in agreement with the calculated electron spin density isosurface (see Supporting Information Table S5 for population analysis).

To further ascertain the existence of the N–H bond in the radical intermediate, we conducted a control experiment with deuterated **1** (Figure 2b). The splitting pattern changed significantly, attributed to the deuteration of the N–H moiety in the imino radical. This observation indicated the presence of the N–H bond in the intermediate. Notably, when enamine **2** without a *tert*-butyl substituent was subjected to TREPR measurement, the resulting spectrum showed a splitting pattern similar to that of **R1** [a(N) = 0.61 mT, a(H) = 0.51 mT,

Citation: *CCS Chem.* **2024**, Just Published. DOI: 10.31635/ccschem.024.202404035
Link to VoR: https://doi.org/10.31635/ccschem.024.202404035

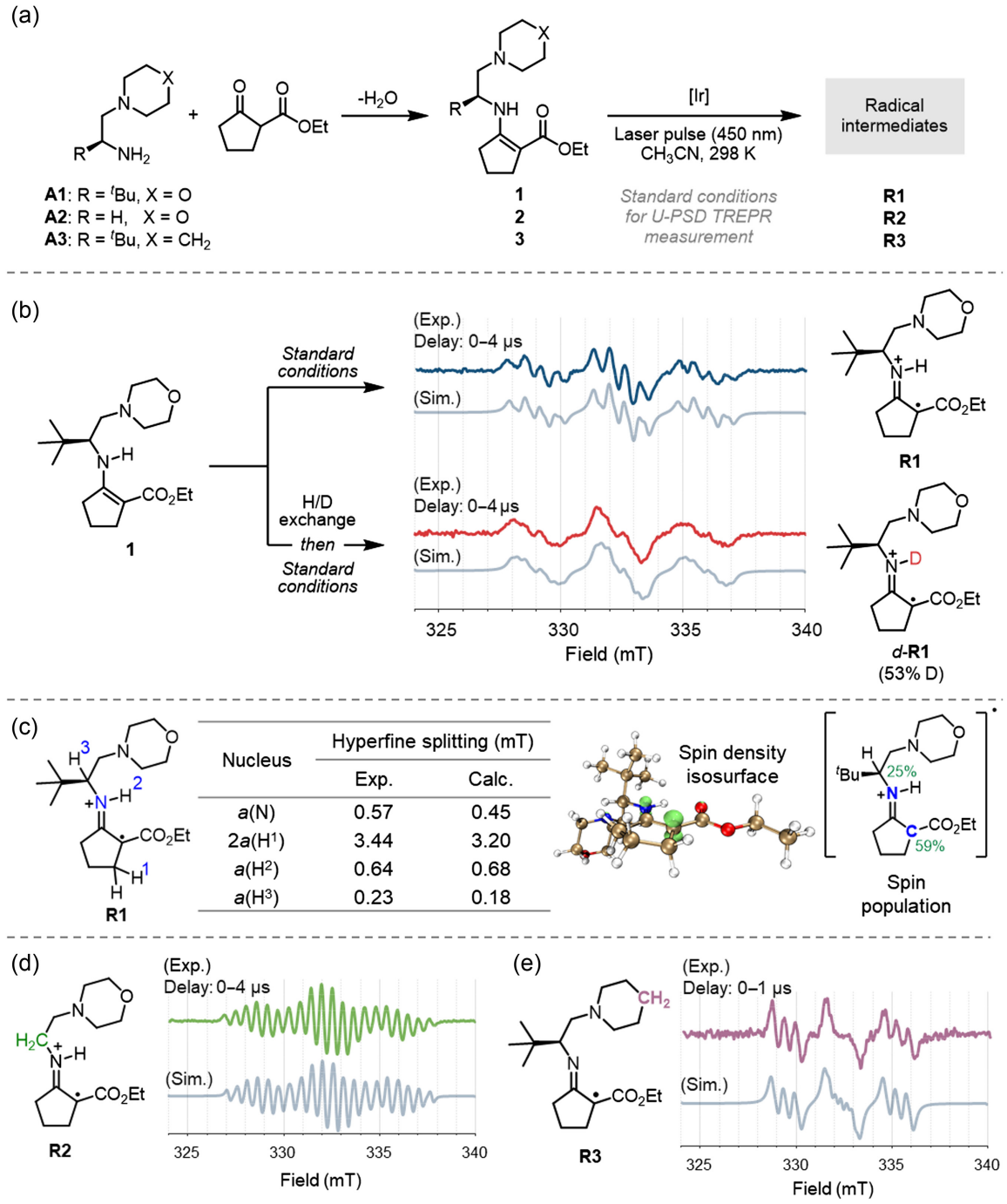

Figure 2 | *Direct observation of the generation of α-imino radical intermediates. (a) The model reactions used in this study. (b) Normal and deuterated **1** (53% D incorporation) gives different TREPR spectra. (c) Fitted and DFT computed HFSs of **R1**. (d) The experimental and simulated TREPR spectra of **R2** derived from **2**. (e) The experimental and simulated TREPR spectra of **R3** derived from **3**. TREPR, time-resolved electron paramagnetic resonance; DFT, density functional theory; HFSs, hyperfine splittings.*

2a(H) = 1.03 mT, 2a(H) = 3.39 mT], except for an extra H^3 in the spin system (Figure 2d, Supporting Information Figure S1). This indicated the generation of radical **R2** that resembled **R1**. Surprisingly, when the tertiary amine moiety in the enamine was switched from morpholine to piperidine, the splitting pattern changed significantly [a(N) = 0.58 mT, a(H) = 0.20 mT, a(H) = 2.76 mT, a(H) = 3.05 mT, Figure 2e]. We have prepared protonated **3** and conducted experiments under standard conditions to obtain the protonated radical, resulting in a spectrum that is different from **R3** (Supporting Information Figure S3). Remarkably, prior to

Citation: *CCS Chem.* **2024**, Just Published. DOI: 10.31635/ccschem.024.202404035
Link to VoR: https://doi.org/10.31635/ccschem.024.202404035

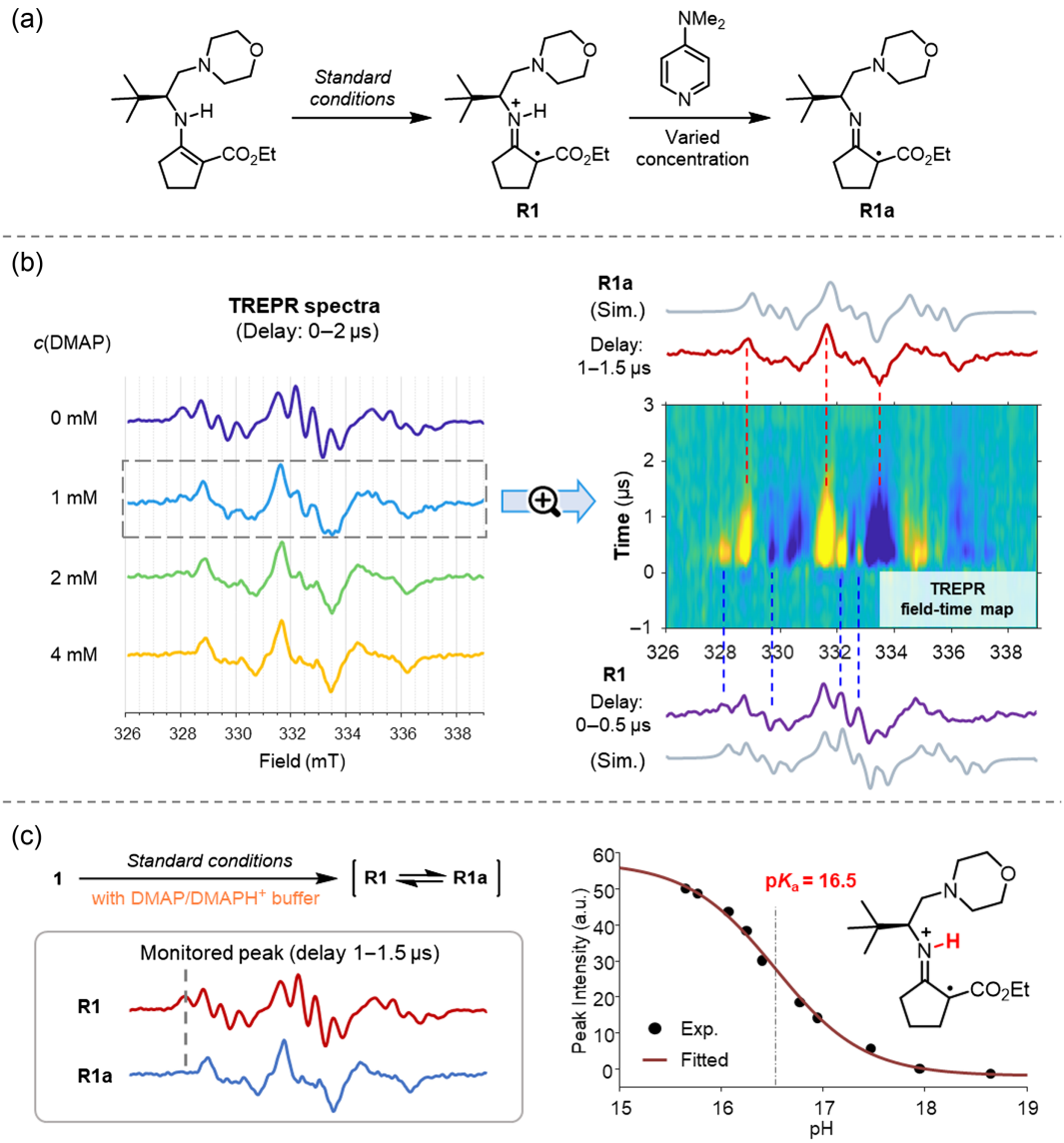

Figure 3 | *(a) Deprotonation of **R1** with DMAP. (b) TREPR spectra with a constant delay (0–2 μs) when different concentrations of DMAP were added to the system (left, four spectra); the field-time map (original instrumental data) when c(DMAP) = 1 mM, with spectra sliced with different time delay (right, one colored contour and two spectra). (c) The titration experiment for the determination of the pK_a of **R1**. DMAP, 4-dimethylaminopyridine; TREPR, time-resolved electron paramagnetic resonance.*

measurement, deuterating enamine **3** did not impact the acquired spectrum of **R3** (Supporting Information Figure S2), contrasting with the behavior observed with **R1**. Hence, we deduced that the disparity arose from the deprotonation of N–H due to the enhanced basicity of the tertiary amine moiety. This finding also pointed to the fact that the pK_a of the enamine radical cation lay between the pK_{aH} of the morpholine (for *N*-methylmorpholine, pK_{aH} = 15.59 in MeCN)[32] and piperidine (for *N*-methylpiperidine, pK_{aH} = 18.24 in MeCN) moieties.[33]

To gain more insight into the deprotonation step, we measured enamine **1** in the presence of an external base, 4-dimethylaminopyridine (DMAP) (Figure 3a). Since its basicity was similar to that of the piperidine moiety (for DMAP, pK_{aH} = 17.95 in MeCN),[34] we envisioned that it could abstract the proton in **R1**. As expected, when the concentration of DMAP increased, we observed a progressive shift in the splitting pattern of the TREPR spectra, transitioning from a spectrum corresponding to **R1** (Figure 3b left, blue spectra) to the one corresponding to deprotonated **R1a** (Figure 3b left, orange spectra). Notably, the spectrum of **R1a** resembled that of **R3** due to the same structural motif of the α-imino radical. Furthermore, the TREPR time-field map measured with 1 mM of DMAP revealed the temporal evolution of the spectrum, corroborating the aforementioned shift (Figure 3b right).

Citation: *CCS Chem.* **2024**, Just Published. DOI: 10.31635/ccschem.024.202404035
Link to VoR: https://doi.org/10.31635/ccschem.024.202404035

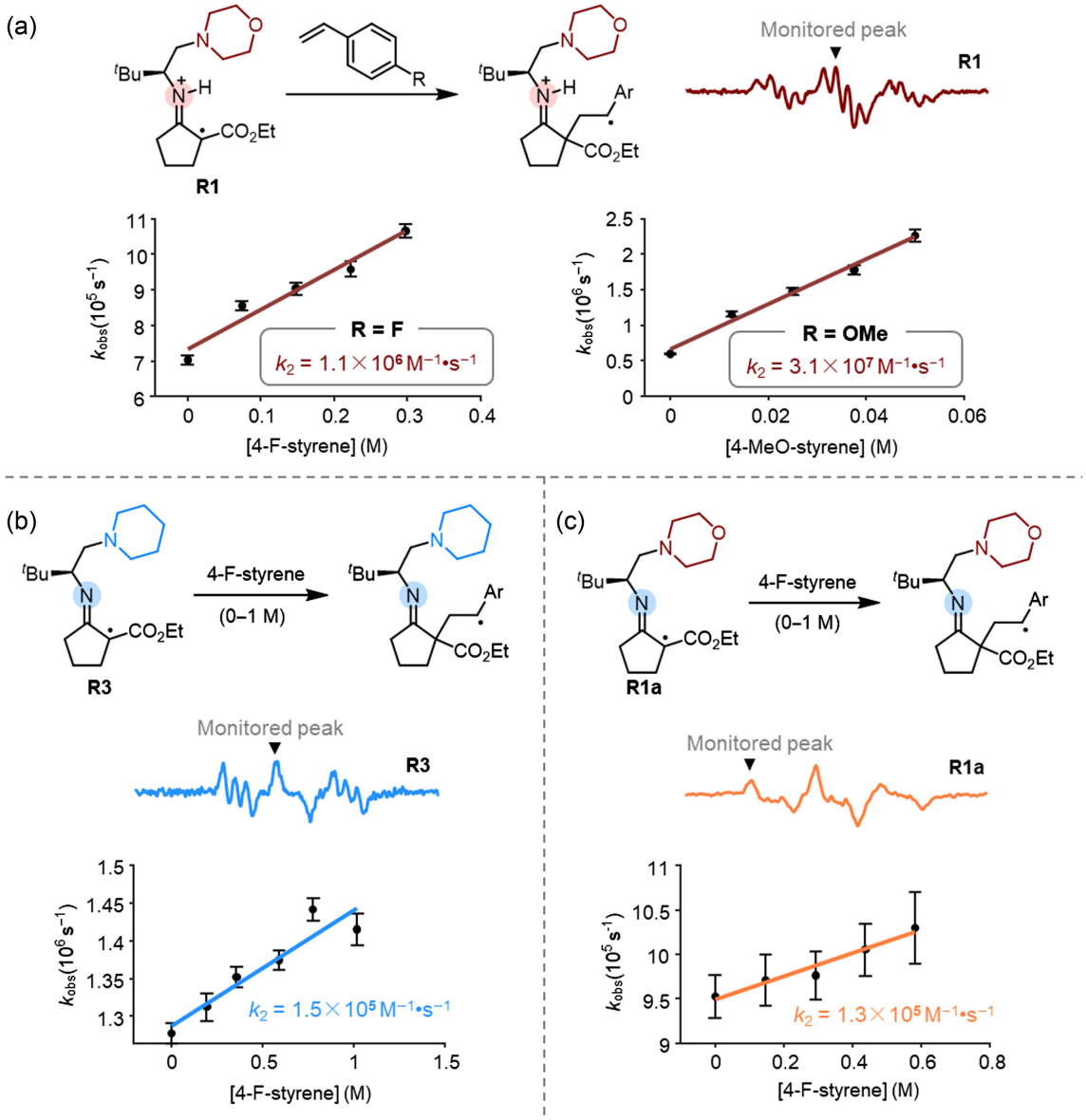

Figure 4 | *Quenching kinetics of α-imino radicals reveals the reactivity difference between **R1**, **R3**, and **R1a**. (a) Kinetic data for **R1**. (b) Kinetic data for **R3**. (c) Kinetic data for **R1a**.*

The half-lifetime of **R1** under this condition was ~100 ns (corresponding to a k_2 of ~6 × 10^9 $M^{-1}s^{-1}$), suggesting a diffusion-controlled deprotonation. This rapid deprotonation process also accounts for the direct formation of **R3** when enamine **3** was employed. Furthermore, the U-PSD TREPR method enabled the determination of the pK_a value of radical cation **R1** through a titration-type experiment (Figure 3c, Supporting Information Figure S5). The formation of radicals via photoinduced SET process from **1** was conducted in the presence of a buffer containing DMAP and the protonated form, $DMAPH^+$. By correlating the acquired peak intensity with the acidity of the buffer solution, a well-fitted titration curve was generated, revealing that the pK_a of radical **R1** was 16.5 in MeCN, consistent with the initial estimation.

The aforementioned results enabled us to further evaluate the reactivity of **R1** and **R3**. We employed 4-fluorostyrene (**4**) as a trapping agent for both radical species and monitored their decay at varying concentrations of **4** (see Supporting Information Tables S1–S4 and Figure S4 for details). The obtained bimolecular rate constants of the reactions between **R1/R3** and **4** revealed that **R1** reacted with **4** at one order of magnitude faster compared to **R3** (Figure 4). This agreed with the consensus that electron-deficient radicals react faster with electron-rich alkenes due to enhanced polarity match.[35] In a subsequent kinetic study involving **R1** and the more electron-rich 4-MeO-styrene (**5**), we found that the electron-rich olefin reacted more rapidly than the electron-deficient one (Figure 4a, right), supporting the

Citation: *CCS Chem.* **2024**, Just Published. DOI: 10.31635/ccschem.024.202404035
Link to VoR: https://doi.org/10.31635/ccschem.024.202404035

aforementioned polarity match. Notably, when **R1** was converted in situ to **R1a** in the presence of excess DMAP (10 mM), the determined quenching kinetics was consistent with that of **R3** (Figure 4b,c), providing further evidence that the enamine radical cation shows greater reactivity than the α-imino radical towards styrene.

The observed difference in reactivity implied that in the photoredox catalytic reaction of secondary enamines, the enamine radical cation (e.g. **R1** at its protonated status) was the key reaction intermediate in the radical addition to styrenes. We previously observed that morphine-derived primary amine catalyst **A1** performed much better than piperidine-derived catalyst **A3** in the reaction shown in Figure 1b, with the product yields being 86% and <5%, respectively.[24] The present study has provided a plausible rationalization of this finding and highlighted the important role of proton transfer in this type of radical reaction. This direct observation of transient radical species in the photoredox catalysis involving enamines grants us deeper mechanistic insights that hold immense promise for the rational design of radical-mediated catalysis.

Supporting Information

Supporting Information is available and includes details for experimental procedures, spectra simulation, kinetic fitting, and compound characterization (PDF).

Conflict of Interest

There is no conflict of interest to report.

Funding Information

We acknowledge the financial support of this work provided by the Tsinghua University Dushi Program, China, the National Natural Science Foundation of China (grant nos. 22031006, 22193011, 22373056, and 22393891), the Haihe Laboratory of Sustainable Chemical Transformations, China, and the National Science & Technology Fundamental Resource Investigation Program of China (grant no. 2023YFA1500008).

Preprint Statement

The corresponding preprint article can be found here: DOI: https://doi.org/10.26434/chemrxiv-2024-r7hxq

References

1. Donslund, B. S.; Johansen, T. K.; Poulsen, P. H.; Halskov, K. S.; Jørgensen, K. A. The Diarylprolinol Silyl Ethers: Ten Years After. *Angew. Chem. Int. Ed.* **2015**, *54*, 13860–13874.
2. Li, J.-L.; Liu, T.-Y.; Chen, Y.-C. Aminocatalytic Asymmetric Diels–Alder Reactions via HOMO Activation. *Acc. Chem. Res.* **2012**, *45*, 1491–1500.
3. Xu, L.-W.; Luo, J.; Lu, Y. Asymmetric Catalysis with Chiral Primary Amine-Based Organocatalysts. *Chem. Commun.* **2009**, *14*, 1807–1821.
4. Beeson, T. D.; Mastracchio, A.; Hong, J.-B.; Ashton, K.; MacMillan, D. W. C. Enantioselective Organocatalysis Using SOMO Activation. *Science* **2007**, *316*, 582–585.
5. Wilson, J. E.; Casarez, A. D.; MacMillan, D. W. C. Enantioselective Aldehyde α-Nitroalkylation via Oxidative Organocatalysis. *J. Am. Chem. Soc.* **2009**, *131*, 11332–11334.
6. Amatore, M.; Beeson, T. D.; Brown, S. P.; MacMillan, D. W. C. Enantioselective Linchpin Catalysis by SOMO Catalysis: An Approach to the Asymmetric α-Chlorination of Aldehydes and Terminal Epoxide Formation. *Angew. Chem. Int. Ed.* **2009**, *48*, 5121–5124.
7. Mastracchio, A.; Warkentin, A. A.; Walji, A. M.; MacMillan, D. W. C. Direct and Enantioselective α-Allylation of Ketones via Singly Occupied Molecular Orbital (SOMO) Catalysis. *Proc. Natl. Acad. Sci. U.S.A.* **2010**, *107*, 20648–20651.
8. Van Humbeck, J. F.; Simonovich, S. P.; Knowles, R. R.; MacMillan, D. W. C. Concerning the Mechanism of the $FeCl_3$-Catalyzed α-Oxyamination of Aldehydes: Evidence for a Non-SOMO Activation Pathway. *J. Am. Chem. Soc.* **2010**, *132*, 10012–10014.
9. Um, J. M.; Gutierrez, O.; Schoenebeck, F.; Houk, K. N.; MacMillan, D. W. C. Nature of Intermediates in Organo-SOMO Catalysis of α-Arylation of Aldehydes. *J. Am. Chem. Soc.* **2010**, *132*, 6001–6005.
10. Pham, P. V.; Ashton, K.; MacMillan, D. W. C. The Intramolecular Asymmetric Allylation of Aldehydes via Organo-SOMO Catalysis: A Novel Approach to Ring Construction. *Chem. Sci.* **2011**, *2*, 1470–1473.
11. Capacci, A. G.; Malinowski, J. T.; McAlpine, N. J.; Kuhne, J.; MacMillan, D. W. C. Direct, Enantioselective α-Alkylation of Aldehydes Using Simple Olefins. *Nat. Chem.* **2017**, *9*, 1073–1077.
12. Bahamonde, A.; Melchiorre, P. Mechanism of the Stereoselective α-Alkylation of Aldehydes Driven by the Photochemical Activity of Enamines. *J. Am. Chem. Soc.* **2016**, *138*, 8019–8030.
13. Næsborg, L.; Corti, V.; Leth, L. A.; Poulsen, P. H.; Jørgensen, K. A. Catalytic Asymmetric Oxidative γ-Coupling of α,β-Unsaturated Aldehydes with Air as the Terminal Oxidant. *Angew. Chem. Int. Ed.* **2018**, *57*, 1606–1610.
14. Næsborg, L.; Leth, L. A.; Reyes-Rodríguez, G. J.; Palazzo, T. A.; Corti, V.; Jørgensen, K. A. Direct Enantio- and Diastereoselective Oxidative Homocoupling of Aldehydes. *Chem.-Eur. J.* **2018**, *24*, 14844–14848.
15. Blom, J.; Reyes-Rodríguez, G. J.; Tobiesen, H. N.; Lamhauge, J. N.; Iversen, M. V.; Barløse, C. L.; Hammer, N.; Rusbjerg, M.; Jørgensen, K. A. Umpolung Strategy for α-Functionalization of Aldehydes for the Addition of Thiols and Other Nucleophiles. *Angew. Chem. Int. Ed.* **2019**, *58*, 17856–17862.
16. Rezayee, N. M.; Enemærke, V. J.; Linde, S. T.; Lamhauge, J. N.; Reyes-Rodríguez, G. J.; Jørgensen, K. A.; Lu, C.; Houk, K.

N. An Asymmetric S_N2 Dynamic Kinetic Resolution. *J. Am. Chem. Soc.* **2021**, *143*, 7509–7520.
17. Graham, T. H.; Jones, C. M.; Jui, N. T.; MacMillan, D. W. C. Enantioselective Organo-Singly Occupied Molecular Orbital Catalysis: The Carbo-Oxidation of Styrenes. *J. Am. Chem. Soc.* **2008**, *130*, 16494–16495.
18. Nicolaou, K. C.; Reingruber, R.; Sarlah, D.; Bräse, S. Enantioselective Intramolecular Friedel–Crafts-Type α-Arylation of Aldehydes. *J. Am. Chem. Soc.* **2009**, *131*, 2086–2087.
19. Wang, D.; Zhang, L.; Luo, S. Enantioselective Decarboxylative α-Alkynylation of β-Ketocarbonyls via a Catalytic α-Imino Radical Intermediate. *Org. Lett.* **2017**, *19*, 4924–4927.
20. Zhu, L.; Wang, D.; Jia, Z.; Lin, Q.; Huang, M.; Luo, S. Catalytic Asymmetric Oxidative Enamine Transformations. *ACS Catal.* **2018**, *8*, 5466–5484.
21. Lin, Q.; Li, L.; Luo, S. Asymmetric Electrochemical Catalysis. *Chem.-Eur. J.* **2019**, *25*, 10033–10044.
22. Li, Y.; Zhang, L.; Luo, S. Bond Energies of Enamines. *ACS Omega* **2022**, *7*, 6354–6374.
23. Zhang, Q.; Shi, M.; Mi, X.; Luo, S. Catalytic Asymmetric Oxidative Sulfenylation of β-Ketocarbonyls Using a Chiral Primary Amine. *Org. Chem. Front.* **2022**, *9*, 1276–1281.
24. Jia, Z.; Zhang, L.; Luo, S. Asymmetric C–H Dehydrogenative Allylic Alkylation by Ternary Photoredox-Cobalt-Chiral Primary Amine Catalysis Under Visible Light. *J. Am. Chem. Soc.* **2022**, *144*, 10705–10710.
25. He, Y.-M.; Cheng, Y.-Z.; Duan, Y.; Zhang, Y.-D.; Fan, Q.-H.; You, S.-L.; Luo, S.; Zhu, S.-F.; Fu, X.-F.; Zhou, Q.-L. Recent Progress of Asymmetric Catalysis from a Chinese Perspective. *CCS Chem.* **2023**, *5*, 2685–2716.
26. Huang, M.; Jia, Z.; Luo, S.; Cheng, J.-P. Quantitative Thermo-Dynamic and Kinetic Parameters of Radical. *Chin. J. Org. Chem.* **2021**, *41*, 3892–3902.
27. Xiao, X.; Xu, K.; Gao, Z.-H.; Zhu, Z.-H.; Ye, C.; Zhao, B.; Luo, S.; Ye, S.; Zhou, Y.-G.; Xu, S.; Zhu, S.-F.; Bao, H.; Sun, W.; Wang, X.; Ding, K. Biomimetic Asymmetric Catalysis. *Sci. China Chem.* **2023**, *66*, 1553–1633.
28. Beel, R.; Kobialka, S.; Schmidt, M. L.; Engeser, M. Direct Experimental Evidence for an Enamine Radical Cation in SOMO Catalysis. *Chem. Commun.* **2011**, *47*, 3293–3295.
29. Zhang, S.; Zhou, S.; Qi, J.; Jiao, L.; Guo, X. Time-Resolved Electron Paramagnetic Resonance Spectrometer Based on Ultrawide Single-Sideband Phase-Sensitive Detection. *Rev. Sci. Instrum.* **2023**, *94*, 084101.
30. Fessenden, R. W.; Schuler, R. H. Electron Spin Resonance Studies of Transient Alkyl Radicals. *J. Chem. Phys.* **1963**, *39*, 2147–2195.
31. Forbes, M. D. E.; Jarocha, L. E.; Sim, S.; Tarasov, V. F. In *Advances in Physical Organic Chemistry*; Williams, I. H.; Williams, N. H., Eds.; North Carolina, USA, **2013**; Vol. 47, pp 1–83.
32. Beltrame, P.; Gelli, G.; Loi, A. Potentiometric Study of the Ionisation of Some Nitrogen Bases in Acetonitrile. *Gazz. Chim. Ital.* **1980**, *110*, 491–494.
33. Tshepelevitsh, S.; Kütt, A.; Lõkov, M.; Kaljurand, I.; Saame, J.; Heering, A.; Plieger, P. G.; Vianello, R.; Leito, I. On the Basicity of Organic Bases in Different Media. *Eur. J. Org. Chem.* **2019**, *2019*, 6735–6748.
34. Kaljurand, I.; Kütt, A.; Sooväli, L.; Rodima, T.; Mäemets, V.; Leito, I.; Koppel, I. A. Extension of the Self-Consistent Spectrophotometric Basicity Scale in Acetonitrile to a Full Span of 28 pK_a Units: Unification of Different Basicity Scales. *J. Org. Chem.* **2005**, *70*, 1019–1028.
35. Tedder, J. M.; Walton, J. C. The Kinetics and Orientation of Free-Radical Addition to Olefins. *Acc. Chem. Res.* **1976**, *9*, 183–191.

Citation: *CCS Chem.* **2024**, Just Published. DOI: 10.31635/ccschem.024.202404035
Link to VoR: https://doi.org/10.31635/ccschem.024.202404035